

Capacity-Oriented Envelope Correlation Coefficient for Multiple Antennas of Mobile Devices

Xide Mei and Ke-Li Wu^{id}, *Fellow, IEEE*

Abstract—In this article, a capacity-oriented envelope correlation coefficient (ECC) that incorporates a preferred channel model for assessing a multiple antenna system of a multiple-input-multiple-output (MIMO) mobile device is proposed. Originated from the rudimentary law of ergodic channel capacity, the ECC for multiple antennas (ECC-M) is proven to holistically reflect the impact of radiation patterns and total efficiencies of multiple antennas on channel capacity. The closed-form ECC-M expressions for Rayleigh fading channel model and ray-based spatial channel model are studied, leading to an easy-to-use ECC-M expression that approximately incorporates a realistic channel model. The correlation of the proposed ECC-M to the channel capacity is demonstrated through the Monte Carlo (MC) simulation of three four-element MIMO antenna testbeds in two channel models, showing that the antenna total efficiency and a realistic channel model involved in the ECC-M play an important role in assessing the performance of multiple antennas. It is justified that the difference in channel capacities of two multiple antenna systems is highly relevant to their ECC-Ms at high signal-to-noise ratios (SNRs). The proposed ECC-M is also experimentally validated through over-the-air (OTA) throughput measurement, revealing that the ECC-M can effectively assess the OTA performance of multiple antenna systems for MIMO terminal devices.

Index Terms—Envelope correlation coefficient (ECC), multiple antennas, multiple-input-multiple-output (MIMO), system performance.

I. INTRODUCTION

IN most of the advanced wireless networks today, the multiple-input-multiple-output (MIMO) technology [1] has become a compulsory means to increase the system data throughput by transmitting data streams in multiple relatively uncorrelated wireless channels. The assessment of over-the-air (OTA) performance of an MIMO wireless device is critical to assess the ultimate data transmission quality that depends on not only the wireless channel properties, channel precoding schemes, but also the design of the multiple antennas of the mobile device. Many valuable works are focused on proposing simple and cost-effective methods for antenna designers to relate the antenna passive measurement results to the overall OTA performance. Several figures of merit to assess the performance of multiple antennas for mobile devices are available in the literature.

Manuscript received 16 January 2022; revised 11 May 2022; accepted 28 May 2022. Date of publication 24 June 2022; date of current version 9 November 2022. This work was supported by the Postgraduate Scholarship of The Chinese University of Hong Kong. (*Corresponding author: Ke-Li Wu.*)

The authors are with the Department of Electronic Engineering, The Chinese University of Hong Kong, Shatin, Hong Kong (e-mail: xdmei@link.cuhk.edu.hk; kluw@cuhk.edu.hk).

Color versions of one or more figures in this article are available at <https://doi.org/10.1109/TAP.2022.3184541>.

Digital Object Identifier 10.1109/TAP.2022.3184541

1) Envelope correlation coefficient (ECC) [2] was proposed in 1987 to address the pattern correlation of two antennas in terms of covariance that influences the diversity gain of a mobile device using multiple antennas [3]. Although the origin of its deduction is imperceptible, ECC is most widely used by antenna designers to assess a two-antenna system for a multiplexing scheme [4]. Numerical analysis of ECC of two dipole antennas in a nonuniform propagation environment is also investigated in [5] and [6]. The main limitations of ECC include restriction to two-element antenna arrays in Rayleigh channel environment and its exclusion of antenna efficiencies.

2) The multiplexing efficiency [7] is a simple and intuitive metric that depends on signal-to-noise ratio (SNR) for evaluating the performance of MIMO antennas under the assumption of Kronecker Rayleigh channel model [8]. By introducing the receive correlation matrix \mathbf{R} , the general mobile channel matrix \mathbf{H} is bluntly replaced by $\mathbf{R}^{1/2}\mathbf{H}_W$, where \mathbf{H}_W is the Rayleigh fading channel matrix. The metric lacks a theoretic correlation with channel capacity in a realistic channel model.

3) The data throughput of OTA measurement in a realistic channel environment [9]–[11] or simulation [12], [13] is the most admissible figure of merit to assess the ultimate performance of a mobile device with multiple antennas. However, a setup of a realistic channel environment involving a large number of random variables is very costly. The simulation approaches have to involve Monte Carlo (MC) simulation, which is not straightforward for antenna designers.

Having said that, a simple-to-use and physically meaningful description of a multiple antenna system (more than two elements) with regard to OTA MIMO performance is highly needed for antenna designers.

In this article, a new figure of merit—capacity-oriented ECC for multiple antennas or ECC-M—is proposed for a quick assessment of a multiple antenna design with consideration of a preferred channel model. The definition of the ECC-M is originated from the rudimentary law of ergodic channel capacity and is deduced rigorously by applying five sensible assumptions and approximations to the accurate statistical representation of ergodic channel capacity. It will be shown that ECC-M is a constant, which not only depends on the radiation patterns and total efficiencies of the multiple antennas but also on the channel environment in which the mobile device operates. As a special case, the normalized ECC-M (ECC-M_n) is also given for which the antenna efficiency-related terms are suppressed. The ECC-M_n is a more general case of the conventional ECC. It will be seen that the importance of involving the characteristic of a realistic channel model which is generally ignored in traditional ECC. For a

practical use of the proposed ECC-M with a ray-based realistic channel model, a closed-form approximate incoming wave distribution of a third Generation Partnership Project (3GPP) standardized nonuniformed channel model is introduced. It needs to mention that the work in this article is a substantial evolution of [14], in which an ECC for multiple lossless antennas in the Rayleigh channel was proposed without rigorously justifying the correspondence with the channel capacity.

To demonstrate the usefulness of the proposed ECC-M, three testbeds with four antenna elements are built and radiation patterns are measured. MC simulations of the validation examples show that ECC-M values are consistent with the simulated ergodic channel capacities as far as the radiation patterns, total efficiencies, and antenna placements are concerned and that ECC-M is asymptotically related to the channel capacity as the SNR increases. The examples also demonstrate the importance of considering a realistic channel model in the proposed ECC-M. Furthermore, the experimental OTA throughput validation is also carried out, showing that ECC-M is consistent with the OTA data throughput.

This article is arranged as follows: the derivation of ECC-M is first presented in Section II, which includes the representation of a realistic channel model, the simplification of the channel model, legitimate assumptions, and mathematic representations of ECC-M. The physical meaning of the concerned matrix that defines ECC-M with respect to a specific channel model is discussed in Section III. Simulation-based validation examples with three four-antenna testbeds are presented in Section IV followed by experimental validation with measured OTA data throughput in a multiprobe anechoic chamber (MPAC). Finally, a brief conclusion is given in Section V.

II. THEORY

Enormous works have been done to study the channel capacity [15]–[17] for a multiple antenna MIMO system. The ergodic channel capacity is formulated as

$$\bar{C} = E_{\mathbf{H}} \left\{ \log_2 \det \left(\mathbf{I} + \frac{\mathbf{H}\mathbf{H}^\dagger}{N_t} \text{SNR} \right) \right\} \quad (1)$$

where $E_{\mathbf{H}}\{\cdot\}$ denotes the expectation with respect to the mobile channel \mathbf{H} with N_r by N_t entries, in which N_t is the number of transmitting antennas and N_r is the number of the receiving antennas, \mathbf{I} is an identity matrix of N_r by N_r , SNR is the signal to noise ratio, $\det(\cdot)$ denotes the determinant operation, and $(\cdot)^\dagger$ denotes the Hermitian operation. In this study, the base station antennas are transmitting antennas and antennas on a mobile device are considered as receiving antennas.

Instead of using (1) directly in a theoretical simulation that may involve MC simulation, using Jensen's inequality, the channel capacity can be estimated by its upper bound approximation as [7]

$$\bar{C} \leq \log_2 \det \left(\mathbf{I} + \frac{E_{\mathbf{H}}\{\mathbf{H}\mathbf{H}^\dagger\}}{N_t} \text{SNR} \right) = \bar{C}_A. \quad (2)$$

It can be seen from (2) that for a high SNR, the channel capacity is dominated by $E_{\mathbf{H}}\{\mathbf{H}\mathbf{H}^\dagger\}$, and thus, the focus of this work will be placed on the description of the channel matrix $E_{\mathbf{H}}\{\mathbf{H}\mathbf{H}^\dagger\}$ and its simplification.

A. Description of the Channel Matrix

There are different types of channel models that describe the statistical phenomena of electromagnetic waves traveling through different environments. Mobile devices in most of cases operate in a rich multipath environment. The channel matrix of such an environment can be written as the summation of the waves with different subpaths as follows [18]:

$$\mathbf{H} = \sum_{i=1}^M \begin{bmatrix} H_{11,i} & H_{12,i} & \cdots & H_{1N_r,i} \\ H_{21,i} & H_{22,i} & \cdots & H_{2N_r,i} \\ \vdots & \vdots & \ddots & \vdots \\ H_{N_r,1,i} & H_{N_r,2,i} & \cdots & H_{N_r,N_r,i} \end{bmatrix} \quad (3)$$

where $H_{n_r n_t, i}$ represents the channel coefficient between the n_r th receiving antenna and the n_t th transmitting antenna for the i th subpath in a communication link, and M is the number of the subpaths that is determined by the scatters in the environment and equals around 20 for a rich scattering environment [10]. According to Friis's transmission theory, the received power is proportional to the radiation patterns of the transmitting and the receiving antennas and the channel coefficient between the transmitter and receiver. The channel coefficient of a ray-based channel model can be written as [18]

$$H_{n_r n_t, i} = \mathbf{E}_{n_t}^T(\Theta_{AOD,i}) \mathbf{T}_{n_t n_r, i} \mathbf{E}_{n_r}(\Theta_{AOA,i}) \quad (4)$$

where $\mathbf{E}_{n_t}(\Theta_{AOD})$ is the electrical field of the n_t th transmitting antenna in the i th subpath in the direction of $\Theta_{AOD,i}$ (angle of departure or AOD), $\mathbf{E}_{n_r}(\Theta_{AOA})$ is the electrical field of the n_r th transmitting antenna in the i th subpath in the direction of $\Theta_{AOA,i}$ (angle of arrival or AOA), $\mathbf{T}_{n_t n_r, i}$ is the channel transmission coefficient brought by the scattering and reflection effects in the wireless channel between the n_t th transmitting antenna and the n_r th receiving antenna for the i th subpath, and $(\cdot)^T$ denotes the transpose expression. The electric fields of the transmitting and receiving antennas can be further detailed by the antenna gains of θ and φ field components. Specifically, the detailed information in (4) can be written in terms of antenna radiation patterns and ray-based channel properties. Therefore, (4) can be reformulated as

$$\begin{aligned} \mathbf{T}_{n_t n_r, i} &= \begin{bmatrix} \sqrt{1 - \Gamma_{1,i}^2} h_{n_r n_t, i}^{\theta\theta} & \Gamma_{1,i} h_{n_r n_t, i}^{\theta\varphi} \\ \Gamma_{2,i} h_{n_r n_t, i}^{\varphi\theta} & \sqrt{1 - \Gamma_{2,i}^2} h_{n_r n_t, i}^{\varphi\varphi} \end{bmatrix} \\ \mathbf{E}_{n_t}(\Theta_{AOD,i}) &= \begin{bmatrix} E_{n_t}^\theta(\Theta_{AOD,i}) \\ E_{n_t}^\varphi(\Theta_{AOD,i}) \end{bmatrix} \\ &= \left\langle \frac{\sqrt{G_{n_t}^\theta(\Theta_{AOD,i})} \exp[j\phi_{n_t}^\theta(\Theta_{AOD,i})]}{\sqrt{G_{n_t}^\varphi(\Theta_{AOD,i})} \exp[j\phi_{n_t}^\varphi(\Theta_{AOD,i})]} \right\rangle \\ \mathbf{E}_{n_r}(\Theta_{AOA,i}) &= \begin{bmatrix} E_{n_r}^\theta(\Theta_{AOA,i}) \\ E_{n_r}^\varphi(\Theta_{AOA,i}) \end{bmatrix} \\ &= \left\langle \frac{\sqrt{G_{n_r}^\theta(\Theta_{AOA,i})} \exp[j\phi_{n_r}^\theta(\Theta_{AOA,i})]}{\sqrt{G_{n_r}^\varphi(\Theta_{AOA,i})} \exp[j\phi_{n_r}^\varphi(\Theta_{AOA,i})]} \right\rangle \end{aligned} \quad (5)$$

where $G_{n_i}^{\theta,\varphi}(\Theta_{AOD,i})$ and $\phi_{n_i}^{\theta,\varphi}(\Theta_{AOD,i})$ are the gains and phases of the n_i th transmitting antenna at angle $\Theta_{AOD,i}$ of the i th path of \mathbf{e}_θ and \mathbf{e}_φ field components, respectively; $G_{n_r}^{\theta,\varphi}(\Theta_{AOA,i})$ and $\phi_{n_r}^{\theta,\varphi}(\Theta_{AOA,i})$ are the gains and phases of the n_r th transmitting antenna at angle $\Theta_{AOA,i}$ of the i th path of \mathbf{e}_θ and \mathbf{e}_φ field components, respectively; $\Gamma_{1,i}$ and $\Gamma_{2,i}$ are the transmission coefficients of the \mathbf{e}_θ to \mathbf{e}_φ components and the transmission coefficients of the \mathbf{e}_φ to \mathbf{e}_θ components of the i th path, respectively; $h_{n_r,n_i,i}^{\theta\theta}$, $h_{n_r,n_i,i}^{\varphi\varphi}$, $h_{n_r,n_i,i}^{\theta\varphi}$, and $h_{n_r,n_i,i}^{\varphi\theta}$ are the inherent fading channel parameters for the i th path of the \mathbf{e}_θ and \mathbf{e}_φ field components; and $\langle \cdot \rangle$ represents a vector. Thus, the channel coefficient in (4) can be expanded as

$$\begin{aligned} H_{n_r,n_i,i} &= \Gamma_{1,i} E_{n_i}^\varphi(\Theta_{AOD,i}) E_{n_r}^\theta(\Theta_{AOA,i}) h_i^{\varphi\theta} \\ &\quad + \Gamma_{2,i} E_{n_i}^\theta(\Theta_{AOD,i}) E_{n_r}^\varphi(\Theta_{AOA,i}) h_i^{\theta\varphi} \\ &\quad + \sqrt{1 - \Gamma_{2,i}^2} E_{n_i}^\varphi(\Theta_{AOD,i}) E_{n_r}^\varphi(\Theta_{AOA,i}) h_i^{\varphi\varphi} \\ &\quad + \sqrt{1 - \Gamma_{1,i}^2} E_{n_i}^\theta(\Theta_{AOD,i}) E_{n_r}^\theta(\Theta_{AOA,i}) h_i^{\theta\theta}. \end{aligned} \quad (6)$$

It can be seen from (6) that the coefficient of the channel matrix between the n_i th transmitting antenna and the n_r th receiving antenna depends on the radiation patterns of the antennas on the two sides of the transmission.

Having had (6), $\mathbf{H}\mathbf{H}^\dagger$ can be written as

$$(\mathbf{H}\mathbf{H}^\dagger)_{pq} = \frac{1}{M} \sum_{n_i=1}^{N_i} \left(\sum_{i=1}^M H_{p n_i,i} \sum_{i=1}^M H_{q n_i,i}^* \right) \quad (7)$$

where p and q represent the row and column indexes of matrix $\mathbf{H}\mathbf{H}^\dagger$, respectively.

B. Simplification of Channel Matrix $E_{\mathbf{H}}\{\mathbf{H}\mathbf{H}^\dagger\}$

Direct use of (7) requires much detailed but trivial channel information that may not contribute to $E_{\mathbf{H}}\{\mathbf{H}\mathbf{H}^\dagger\}$ and, consequently, the essence of the OTA performance of an MIMO mobile device significantly. To grasp the essence, some simplifications need to be made based on sensible assumptions. In a rich scattering multipath scenario, the correlation between different paths of transmission is weak, so that the following assumption (*Assumption 1*) can be made [19]:

$$\begin{aligned} E\{h_m^{\theta\theta} h_n^{\theta\theta*}\} &= E\{h_m^{\varphi\varphi} h_n^{\varphi\varphi*}\} = E\{h_m^{\varphi\theta} h_n^{\varphi\theta*}\} \\ &= E\{h_m^{\theta\varphi} h_n^{\theta\varphi*}\} = 0 \quad \text{for } m \neq n \end{aligned} \quad (8)$$

where m and n are the indexes for two different paths between the transmitter and receiver.

There are two types of multiplication terms in $E_{\mathbf{H}}\{\mathbf{H}\mathbf{H}^\dagger\}$ for the same path of transmission: 1) the correlation between different field polarization [18] and 2) the intracorrelation of the same polarization. If the correlation between field polarizations is neglected, the following assumption (*Assumption 2*) can be held [2]:

$$E\{h_m^{\theta\theta} h_m^{\varphi\varphi*}\} = E\{h_m^{\varphi\theta} h_m^{\theta\varphi*}\} = 0. \quad (9)$$

To be consistent with the power-angular distribution of a channel, for a ray-based channel model with M subpaths,

Assumption 3 states that the intracorrelation terms can be written as [20]

$$\begin{aligned} E\{h_1^{\theta\theta} h_1^{\theta\theta*}\} &= E\{h_1^{\varphi\varphi} h_1^{\varphi\varphi*}\} = E\{h_2^{\theta\theta} h_2^{\theta\theta*}\} = E\{h_2^{\varphi\varphi} h_2^{\varphi\varphi*}\} \\ &= \dots = E\{h_M^{\theta\theta} h_M^{\theta\theta*}\} = E\{h_M^{\varphi\varphi} h_M^{\varphi\varphi*}\} = \frac{1}{M}. \end{aligned} \quad (10)$$

It can be justified that if the base station antennas transmit signals with the same magnitude in both polarizations, which is usually true, the components that involve $\Gamma_{1,i}$ and $\Gamma_{2,i}$ in (6) will be canceled each other [2]. As a result, $\Gamma_{1,i}$ and $\Gamma_{2,i}$ are set to zero in this work under the assumption.

Assumption 4 is made about the radiation patterns of the transmitting antennas on base stations. Since the surrounding and element spacing for transmitting antennas are clean and sufficiently large, the spatial correlation (also known as the pattern correlation) can be negligible. Furthermore, to focus on the mobile device antennas, the radiation patterns of the base station antennas are assumed to be omnidirectional in both polarizations, which is described by

$$|E_{n_i}^\theta(\Theta_{AOD,i})| = |E_{n_i}^\varphi(\Theta_{AOD,i})| = 1. \quad (11)$$

Be noted that, in MC simulation, the phase terms of transmitting antennas are determined by an ideal array factor for a given AOD. The distance between antennas is chosen to be half a wavelength to minimize the correlation of the transmitting array.

Under *Assumption 5*, other factors that are not directly related to the radiation patterns of the multiple antennas on the mobile device but may affect the OTA performance, such as the desense effect [21], are neglected. The port isolation is not directly incorporated but is reflected by total efficiencies of the multiple antennas.

C. Introduction to ECC-M

Based on Assumption 1 through Assumption 3, the entries of $E_{\mathbf{H}}\{\mathbf{H}\mathbf{H}^\dagger\}$ can be simplified as

$$\begin{aligned} E_{\mathbf{H}}\{(\mathbf{H}\mathbf{H}^\dagger)_{pq}\} &= \sum_{i=1}^M \sum_{n_i=1}^{N_i} [E\{E_p^\theta(\Theta_{AOA,i}) E_q^{\theta*}(\Theta_{AOA,i})\} \\ &\quad \times E\{E_{n_i}^\theta(\Theta_{AOD,i}) E_{n_i}^{\theta*}(\Theta_{AOD,i})\} \\ &\quad + E\{E_p^\varphi(\Theta_{AOA,i}) E_q^{\varphi*}(\Theta_{AOA,i})\} \\ &\quad \times E\{E_{n_i}^\varphi(\Theta_{AOD,i}) E_{n_i}^{\varphi*}(\Theta_{AOD,i})\}] \end{aligned} \quad (12)$$

where i is the index of an arbitrary subpath. Applying Assumption 4 to (12) leads to a simplified expression that only depends on the properties of the antennas on the mobile device regardless of the base station antennas. Therefore, the pattern correlation of the base station antennas is not considered if the approximation in (2) is applied. In other words, the pattern correlation of the mobile device antennas is more important than that on the base station side. This result is understandable since the antenna separation for the base station antennas is about half a wavelength while that in a mobile device is around 0.2–0.3 wavelength or even less. After applying

Assumptions 3 and 4 to (12), the simplified expression can be as concise as

$$E_{\mathbf{H}}\{(\mathbf{H}\mathbf{H}^\dagger)\}_{pq} = \sum_{n_r=1}^{N_r} \left[E\{E_p^\theta(\Theta_{AOA})E_q^{\theta*}(\Theta_{AOA})\} + E\{E_p^\varphi(\Theta_{AOA})E_q^{\varphi*}(\Theta_{AOA})\} \right] \quad (13)$$

which shows that $E_{\mathbf{H}}\{(\mathbf{H}\mathbf{H}^\dagger)\}$ only depends on the radiated electric fields of the p th and q th mobile device antennas. Equation (13) can be rewritten as, in terms of the probability density function (pdf) $f(\Theta_{AOA})$ of the AOA

$$\begin{aligned} E_{\mathbf{H}}\{E_p^\theta(\Theta_{AOA})E_q^{\theta*}(\Theta_{AOA}) + E_p^\varphi(\Theta_{AOA})E_q^{\varphi*}(\Theta_{AOA})\} \\ = \int_{\theta=0}^{\pi} \int_{\varphi=0}^{2\pi} E_p^\theta(\Theta_{AOA})E_q^{\theta*}(\Theta_{AOA})f(\Theta_{AOA})d\theta d\varphi \\ + \int_{\theta=0}^{\pi} \int_{\varphi=0}^{2\pi} E_p^\varphi(\Theta_{AOA})E_q^{\varphi*}(\Theta_{AOA})f(\Theta_{AOA})d\theta d\varphi. \end{aligned} \quad (14)$$

Denoting $E_{\mathbf{H}}\{(\mathbf{H}\mathbf{H}^\dagger)\}_{pq}$ as ρ_{pq} , which is called correlation coefficient for the antenna pair, $E_{\mathbf{H}}\{(\mathbf{H}\mathbf{H}^\dagger)\}$ can be written in integral form as

$$E_{\mathbf{H}}\{(\mathbf{H}\mathbf{H}^\dagger)\} = \begin{bmatrix} \rho_{11} & \rho_{12} & \cdots & \rho_{1N_r} \\ \rho_{12}^* & \rho_{22} & \cdots & \rho_{2N_r} \\ \vdots & \vdots & \ddots & \vdots \\ \rho_{1N_r}^* & \rho_{2N_r}^* & \cdots & \rho_{N_r N_r} \end{bmatrix}$$

with

$$\rho_{pq} = \int_{\theta=0}^{\pi} \int_{\varphi=0}^{2\pi} \left[E_p^\theta(\Theta_{AOA})E_q^{\theta*}(\Theta_{AOA})f(\Theta_{AOA}) + E_p^\varphi(\Theta_{AOA})E_q^{\varphi*}(\Theta_{AOA})f(\Theta_{AOA}) \right] d\theta d\varphi. \quad (15)$$

In light of (15), the ECC for assessing the performance of a multiple antenna system, namely, ECC-M, can be defined as

$$ECC-M = 1 - \begin{vmatrix} \rho_{11} & \rho_{12} & \cdots & \rho_{1N_r} \\ \rho_{12}^* & \rho_{22} & \cdots & \rho_{2N_r} \\ \vdots & \vdots & \ddots & \vdots \\ \rho_{1N_r}^* & \rho_{2N_r}^* & \cdots & \rho_{N_r N_r} \end{vmatrix} \quad (16)$$

where $|\cdot|$ denotes the determinant of a matrix. After the mathematical transformation, (16) can also be rewritten as

$$ECC-M = 1 - \prod_{n_r=1}^{N_r} \rho_{n_r n_r} \begin{vmatrix} 1 & \frac{\rho_{12}}{\sqrt{\rho_{11}\rho_{22}}} & \cdots & \frac{\rho_{1N_r}}{\sqrt{\rho_{11}\rho_{N_r N_r}}} \\ \frac{\rho_{12}^*}{\sqrt{\rho_{11}\rho_{22}}} & 1 & \cdots & \frac{\rho_{2N_r}}{\sqrt{\rho_{22}\rho_{N_r N_r}}} \\ \vdots & \vdots & \ddots & \vdots \\ \frac{\rho_{1N_r}^*}{\sqrt{\rho_{11}\rho_{N_r N_r}}} & \frac{\rho_{2N_r}^*}{\sqrt{\rho_{22}\rho_{N_r N_r}}} & \cdots & 1 \end{vmatrix}. \quad (17)$$

In view of the definition of ECC for two antennas, in which the antenna efficiency-related terms are denormalized, the normalized version for ECC-M for multiple antennas, namely, ECC-M_n, can be defined as

$$ECC-M_n = 1 - \begin{vmatrix} 1 & \frac{\rho_{12}}{\sqrt{\rho_{11}\rho_{22}}} & \cdots & \frac{\rho_{1N_r}}{\sqrt{\rho_{11}\rho_{N_r N_r}}} \\ \frac{\rho_{12}^*}{\sqrt{\rho_{11}\rho_{22}}} & 1 & \cdots & \frac{\rho_{2N_r}}{\sqrt{\rho_{22}\rho_{N_r N_r}}} \\ \vdots & \vdots & \ddots & \vdots \\ \frac{\rho_{1N_r}^*}{\sqrt{\rho_{11}\rho_{N_r N_r}}} & \frac{\rho_{2N_r}^*}{\sqrt{\rho_{22}\rho_{N_r N_r}}} & \cdots & 1 \end{vmatrix}. \quad (18)$$

It can be seen from (17) and (18), the diagonal terms of the determinant are unitary, and the off-diagonal terms are the original off-diagonal terms in (16) normalized by the diagonal terms. It can be readily proved that the diagonal terms in ECC-M correspond to the total efficiencies of antennas. The major difference between ECC-M and ECC-M_n lies in the antenna total efficiencies. ECC-M takes the pattern correlation and the efficiencies into considerations whereas ECC-M_n does not.

III. DEPENDENCE ON CHANNEL MODEL

Having defined ECC-M and ECC-M_n, it is also intuitive to know the physical meaning of the two figures of merit. As can be seen from (15) that both ECC-M and ECC-M_n highly depend on the chosen channel model. Therefore, the physical meaning of ECC-M and ECC-M_n in different channel model needs to be revealed. Two typical channel models are considered in this work for illustration purposes.

A. Rayleigh Fading Channel

The simplest way to describe the incoming waves is to consider the Rayleigh fading channel, in which the incoming waves are omnidirectionally distributed, mathematically

$$f(\Theta_{AOA}) = f(\theta, \varphi) = \frac{1}{4\pi} \sin\theta \quad \theta \in (0, \pi); \varphi \in (0, 2\pi). \quad (19)$$

There are two conditions for calculating ECC-M: 1) $p = q$ and 2) $p \neq q$. For the case of $p = q$, the correlation coefficient ρ_{pp} in (15) can be written as

$$\rho_{pp} = \frac{1}{4\pi} \int_{\theta=0}^{\pi} \sin\theta d\theta \int_{\varphi=0}^{2\pi} \left[\|E_p^\varphi(\theta, \varphi)\|^2 + \|E_p^\theta(\theta, \varphi)\|^2 \right] d\varphi. \quad (20)$$

In light of (5), the correlation coefficient can be rewritten as

$$\rho_{pp} = \frac{1}{4\pi} \int_{\theta=0}^{\pi} \int_{\varphi=0}^{2\pi} G_p(\theta, \varphi) \sin\theta d\theta d\varphi \quad (21)$$

where $G_p(\theta, \varphi)$ is the antenna gain pattern for the p th antenna. By making use of the relationship between antenna directivity and the antenna gain patterns, (21) can be further rewritten as

$$\rho_{pp} = \frac{1}{4\pi} \eta_p \int_{\theta=0}^{\pi} \int_{\varphi=0}^{2\pi} D_p(\theta, \varphi) \sin\theta d\theta d\varphi = \eta_p \quad (22)$$

where η_p and $D_p(\theta, \varphi)$ are the antenna total efficiency and directivity of the p th antenna, respectively. The simplification process can be easily obtained through the basic definition of the antenna directivity [22]. Clearly, (22) states that the diagonal terms of ECC-M in the Rayleigh fading channel are nothing but the antenna efficiencies of the corresponding antennas.

For the case of $p \neq q$, the correlation coefficient

$$\rho_{pq} = \frac{1}{4\pi} \int_{\theta=0}^{\pi} \int_{\varphi=0}^{2\pi} \left[E_p^\theta(\theta, \varphi) E_q^{\theta*}(\theta, \varphi) + E_p^\varphi(\theta, \varphi) E_q^{\varphi*}(\theta, \varphi) \right] \sin \theta d\theta d\varphi \quad (23)$$

which can be reformulated, in terms of antenna efficiencies, as

$$\rho_{pq} = \sqrt{\eta_p \eta_q} \frac{\int_{\theta=0}^{\pi} \int_{\varphi=0}^{2\pi} \left[E_p^\theta(\theta, \varphi) E_q^{\theta*}(\theta, \varphi) + E_p^\varphi(\theta, \varphi) E_q^{\varphi*}(\theta, \varphi) \right] \sin \theta d\theta d\varphi}{\sqrt{\prod_{n=p \text{ or } q} \int_{\theta=0}^{\pi} \int_{\varphi=0}^{2\pi} \left[\|E_n^\theta(\theta, \varphi)\|^2 + \|E_n^\varphi(\theta, \varphi)\|^2 \right] \sin \theta d\theta d\varphi}} \quad (24)$$

According to the definition of traditional ECC for two antennas [2], the relationship between the correlation coefficient for antenna pairs (p, q) , or ρ_{pq} , and ECC can be written as

$$\rho_{pq} = \sqrt{\eta_p \eta_q} ECC(p, q) \quad (25)$$

where $ECC(p, q)$ represents the ECC between the p th and the q th antennas as defined in [2].

In summary, the proposed ECC-M has a clear physical meaning in the Rayleigh fading channel: the diagonal terms in the matrix describe the total efficiencies of the antennas and the off-diagonal terms describe the pattern correlation of every pair of antennas.

B. SCME Channel Model

When a realistic ray-based channel model is considered, e.g., the 3GPP spatial channel model extension (SCME) channel model [18], specialized forms of (14) through (17) need to be developed. Two typical scenarios in the SCME channel model are the urban microcell (umi) model and the urban macrocell (uma) model, with which there are more than 20 statistic random variables. In the SCME channel model, the delay spread of the received signal is grouped into several independent clusters. For the scenario with six clusters, ρ_{pq} can be written as

$$\rho_{pq} = \sum_{k=1}^6 \int_{P_k=0}^1 \int_{\theta=0}^{\pi} \int_{\varphi=0}^{2\pi} \left[E_p^\theta(\Theta_{AOA}) E_q^{\theta*}(\Theta_{AOA}) f(\Theta_{AOA}, P_k) + E_p^\varphi(\Theta_{AOA}) E_q^{\varphi*}(\Theta_{AOA}) f(\Theta_{AOA}, P_k) \right] \times P_k dP_k d\theta d\varphi \quad (26)$$

where P_k is the normalized power of the k th cluster and $f(\Theta_{AOA}, P_k)$ is the joint pdf of Θ_{AOA} and P_k . Note that Θ_{AOA} and P_k are not independent. To maintain the simplicity of ECC-M, considering the fact that the SCME channel model exhibits an exponential power attenuation versus clusters, the angular power distribution of the major cluster is considered.

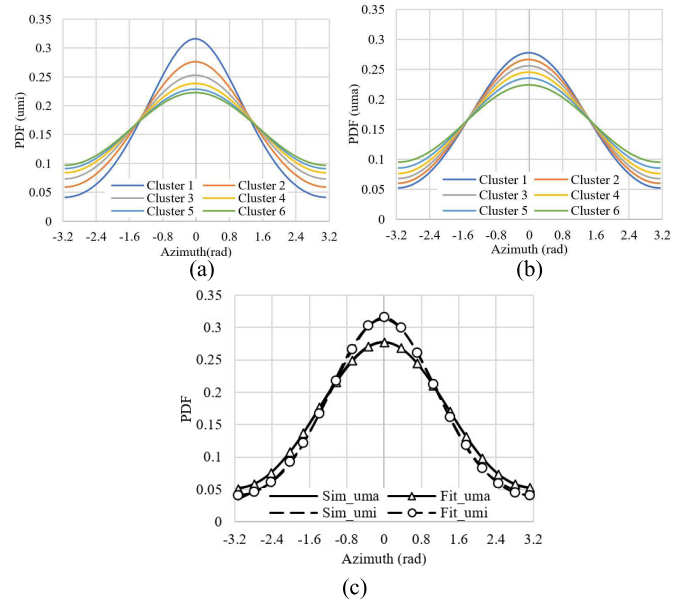


Fig. 1. Pdf of incoming waves of the SCME channel models. (a) umi channel model, (b) uma channel model, and (c) approximate umi and uma models in closed form.

TABLE I
EMPIRICAL FORMULA OF APPROXIMATED PDF
FOR INCOMING WAVES OF SCME MODELS

Scenario	$f_{SCME}(\theta, \varphi)$
umi	$\sin(\theta)[0.129\cos(0.485\varphi)+0.028\cos(1.64\varphi+0.03)]$
uma	$\sin(\theta)[0.109\cos(0.377\varphi)+0.041\cos(1.32\varphi+0.02)]$

Through MC simulation, the distributions of the AOA of each cluster for umi and uma scenarios can be obtained, as shown in Fig. 1(a) and (b). As expected intuitively, the first cluster is most directive than other clusters. Therefore, only the distribution of the first cluster is considered as an appropriate approximation to simplify (26) as

$$\rho_{pq} = \int_{\theta=0}^{\pi} \int_{\varphi=0}^{2\pi} \left[E_p^\theta(\Theta_{AOA}) E_q^{\theta*}(\Theta_{AOA}) f_{SCME}(\Theta_{AOA}) + E_p^\varphi(\Theta_{AOA}) E_q^{\varphi*}(\Theta_{AOA}) f_{SCME}(\Theta_{AOA}) \right] \times d\theta d\varphi \quad (27)$$

where $f_{SCME}(\Theta_{AOA}) = f_{SCME}(\Theta_{AOA}, P_k | P_k=1)$, which is not a function of P_k . To provide an analytical expression of (27), the pdf of the incoming wave of the first cluster can be fitted by an empirical formula. The fitted pdf functions for uma and umi SCME models are listed in Table I. The comparison of the fitted formulas with MC simulation result is shown in Fig. 1(c). Since the SCME is a 2-D channel model, the incoming waves in the elevation plane are not defined. For simplicity, the distribution on the elevation plane can be chosen to be a sine distribution as being used in the Rayleigh fading channel model in the validation examples.

IV. VALIDATION EXAMPLES

To validate the deduction process in Section III and to illustrate the importance of including the channel model, three

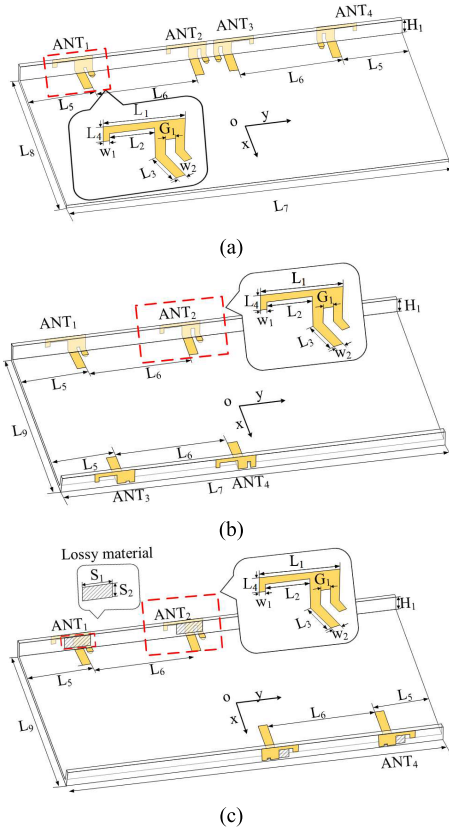


Fig. 2. Schematic views of three testbeds of four IFAs along periphery of the ground board. (a) Case 1, (b) Case 2, and (c) Case 3.

TABLE II
DIMENSIONS FOR THE PROTOTYPED ANTENNA TESTBEDS

	L ₁	L ₂	L ₃	L ₄	L ₅	L ₆	L ₇	L ₈
Dimensions (Unit: mm)	14.1	5.4	10	3	23	60	135	76.6
	L ₉	W ₁	W ₂	G ₁	S ₁	S ₂	H ₁	
	78.2	1.5	3.1	1	4	10	5	

four-antenna testbeds that consist of four inverted F antennas (IFAs) along the long edges of the ground plane that mimics a mobile phone are designed and fabricated, as shown in Fig. 2(a)–(c), which are denoted as Cases 1–3, respectively. A small piece of lossy material is adhered to each antenna in Case 3 for altering antenna efficiency. The dimensions of the sample antennas and the lossy material are listed in Table II. The antennas operate in the frequency range of 3.3–3.8 GHz. The measured S-parameters as well as the antenna efficiencies over the operating frequency band are given in Fig. 3(a)–(c).

Three MC simulation examples based on measured antenna radiation patterns of the three four-antenna testbeds are presented to justify the correlation of ECC-M with channel capacity. In addition, the measured OTA data throughputs of seven two-antenna validation samples are provided to show the consistency of ECC-M and OTA data throughput.

A. Correlation Coefficient

The objective is to study the matrices of $E_H\{\mathbf{H}\mathbf{H}^\dagger\}$ of the four-antenna system in Case 1 obtained by MC simulation

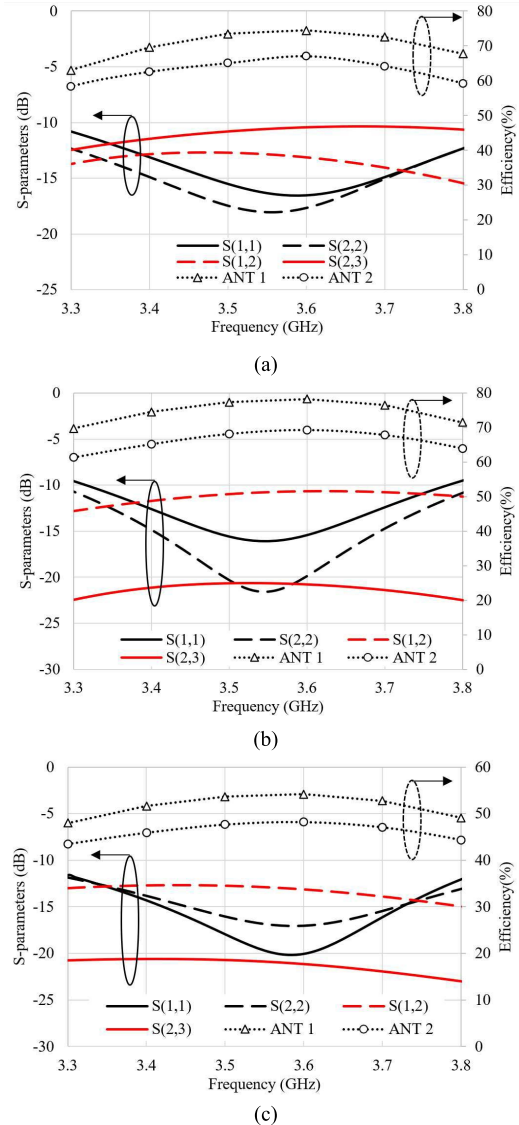


Fig. 3. Measured S-parameters and total efficiencies of the three antenna testbeds for (a)–(c) cases 1–3, respectively.

and the correlation coefficient (15) in integral form in three different channel models: 1) the omnidirectional Rayleigh fading model; 2) the umi SCME model; and 3) the uma SCME model. In the integral form, only the major cluster is considered. The radiation patterns of the four antennas in Case 1 are measured at the center frequency.

The matrices of $E_H\{\mathbf{H}\mathbf{H}^\dagger\}$ for Case 1 by MC simulation and the integral form (15) in the three channel models are presented in Table III. The corresponding ECC-M and ECC-M_n are also given in the table. It can be observed that under the Rayleigh fading channel model, $E_H\{\mathbf{H}\mathbf{H}^\dagger\}$ by MC simulation and (15) is almost the same and that both ECC-M and ECC-M_n by MC simulation and (15) are also nearly the same. This is reasonable because there is no approximation in pdf of AOA. However, under the SCME channel models, the difference of the $E_H\{\mathbf{H}\mathbf{H}^\dagger\}$ by MC simulation and (15) is noticeable, so is ECC-M_n. Since the diagonal terms of $E_H\{\mathbf{H}\mathbf{H}^\dagger\}$, which correspond to the total efficiencies of antennas, dominant and the antenna patterns in Case 1 tend to be omnidirectional,

TABLE III
COMPARISON OF THE CORRELATION COEFFICIENT IN CASE 1 CALCULATED BY MC SIMULATION AND INTEGRATION

Channel	By Monte-Carlo simulation				$ECC-M$ $ECC-M_n$	By Integration				$ECC-M$ $ECC-M_n$
	$E_H\{\mathbf{H}\mathbf{H}^\dagger\}$					$E_H\{\mathbf{H}\mathbf{H}^\dagger\}$				
Rayleigh fading	0.73	0.04+0.01j	-0.03	0.01	0.7812	0.73	0.04+0.02j	-0.03	0.01	0.7816
	0.04-0.01j	0.65	0.11	-0.02		0.04-0.02j	0.65	0.11	-0.03	
	-0.03	0.11	0.65	0		-0.03	0.11	0.65	0	
umi	0.01	-0.02	0	0.73	0.0361	0.01	-0.03	0	0.73	0.0378
	0.79	-0.05-0.11j	0.03j	0.02	0.7550	0.81	-0.09-0.08j	0.04j	0	0.7560
	-0.05+0.11j	0.65	0.1	0		-0.09+0.08j	0.64	0.14	0.01	
-0.03j	0.1	0.65	-0.07+0.05j	-0.04j		0.14	0.64	-0.06+0.04j		
uma	0.02	0	-0.07-0.05j	0.79	0.0707	0	0.01	-0.06-0.04j	0.81	0.0821
	0.74	-0.06-0.03j	-0.01+0.02j	0.02	0.7632	0.73	-0.05-0.07j	-0.02+0.04j	0.02	0.7670
	-0.06+0.02j	0.69	0.08	-0.01		-0.05+0.07j	0.67	0.08	-0.01	
-0.01-0.02j	0.08	0.67	-0.08+0.03j	-0.02-0.04j		0.08	0.68	-0.05+0.02j		
uma	0.02	-0.01	-0.08-0.03j	0.72	0.0386	0.02	-0.01	-0.05-0.02j	0.73	0.0405

the difference in ECC-M values by the two approaches is not significant. Nevertheless, ECC-M_n strongly depends on the channel model. As the number of antennas increases, it is easily found that ECC-M_n for less correlated antennas approaches 0 whereas ECC-M approaches 1.

B. Influence of Channel Model

As revealed by (15), ECC-M highly depends on the channel model. Although the antennas in the three cases shown in Fig. 2 are in the same form, the placements of the antennas are quite different.

The ECC-M in the Rayleigh fading channel, the umi SCME channel whose main incoming wave direction is specified in the x-direction, and the averaged ECC-M in the umi channel by rotating the direction of the incoming waves for every 45° in the horizontal plane, which is in line with the MIMO OTA measurement requirement, are calculated over the operating frequency band. As shown in Fig. 4, under the Rayleigh fading channel model, the calculated ECC-M for Case 3 is the largest, meaning that the performance of Case 3 in terms of the channel capacity is the worst. On the other hand, the smallest ECC-M of Case 2 is with the best performance among the three cases. However, under the umi SCME channel model, the ECC-M for Case 1 is the smallest. Interestingly, the result of the averaged ECC-M under umi SCME channel model is different from those of the Rayleigh fading channel and the umi SCME channel with incoming wave in a specific direction.

Comparing the ECC-M calculated by MC simulation and the integral form shows that: 1) under the Rayleigh fading channel model, two methods give the same result since there is no approximation in the pdf and 2) a little acceptable error is introduced under the umi model in ECC-M using the integral form as compared to that by MC simulation due to the approximation of AOA.

C. Correlation of ECC-M With Channel Capacity

The three testbeds shown in Fig. 2 are also used to validate the relevance between ECC-M and the channel capacity.

Given the good stability of radiation patterns within the frequency band, only the radiation pattern of each antenna at 3.5 GHz is used. Since ECC-M calculated by MC simulation and the integral form have been obtained in Section IV-B, only the ergodic channel capacities in the channel environments are calculated through MC simulation, for which 5000 and 20000 channel samples in time domain for a given SNR are taken under the Rayleigh fading channel and the umi SCME channel models, respectively. The calculated ergodic channel capacities using MC simulation and the upper bound estimation (ES) are presented in Fig. 5(a) and (b), exhibiting the following observations.

- 1) Under the Rayleigh fading channel, the capacity of Case 1 is smaller than Case 2 and both are larger than Case 3, which is consistent with the order of ECC-M shown in Fig. 4(a).
- 2) Under the SCME umi channel, the channel capacity of Case 1 is larger than that of Case 2 and both are larger than Case 3, which is consistent with the order of ECC-M shown in Fig. 4(b).
- 3) Channel capacity varies with the channel model, so does ECC-M.

It can also be noticed that the difference of channel capacities of two different MIMO antenna cases, either calculated by MC simulation or estimated by an upper bound, is nearly the same at high SNRs. This attribute can be interpreted by ECC-M, as at high SNRs, the upper bound ES \bar{C}_A in (2) can be further approximated by

$$\bar{C}_A \approx \bar{C}_{AA} = \log_2 \det \left(\frac{E_H\{\mathbf{H}\mathbf{H}^\dagger\}}{N_t} SNR \right). \quad (28)$$

Then, the difference of \bar{C}_{AA} for case i and case j can be expressed in terms of ECC-M as

$$\begin{aligned} \Delta \bar{C}_{AA}(i, j) &= \bar{C}_{AA}|_{\text{case } i} - \bar{C}_{AA}|_{\text{case } j} \\ &= \log_2 \left(\frac{1 - ECC - M|_{\text{case } i}}{1 - ECC - M|_{\text{case } j}} \right). \end{aligned} \quad (29)$$

It says, at high SNRs, the variation of channel capacity caused by different multiple antenna designs can be well

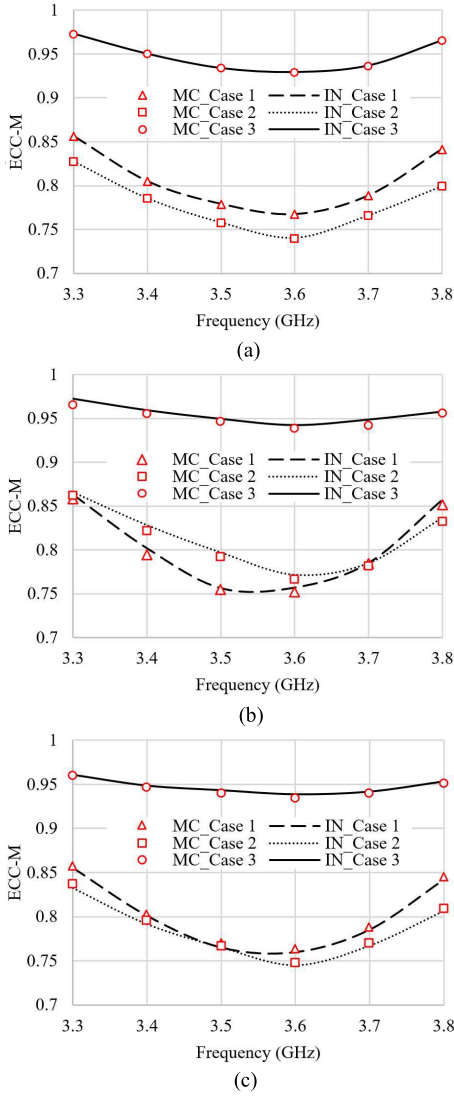


Fig. 4. ECC-M of the three testbed cases under three channel models. (a) Rayleigh fading channel, (b) umi SCME channel (with x-direction incoming wave), and (c) averaged umi SCME channel.

described by ECC-M. The differences of estimated channel capacities \bar{C} , \bar{C}_A , and \bar{C}_{AA} for cases 2 and 3 under the Rayleigh fading and the umi SCME channels are presented in Fig. 6(a) and (b). It is clearly seen that under the Rayleigh fading channel, the differences predicted by \bar{C} and \bar{C}_A are asymptotically approach that by \bar{C}_{AA} , which solely depends on ECC-M according to (29). Under the SCME channel, there is a small gap between the asymptote of \bar{C}_{AA} and that of \bar{C} due to the one AOA cluster assumption made in Section III. Nevertheless, a strong correlation between the variation in channel capacity and ECC-M is clear. This correlation can be used to assess different designs of multiple antennas.

D. Consistency of ECC-M and OTA Data Throughput

The data throughput measurement in a realistic channel environment [9]–[11] is the most direct way to assess the OTA performance of MIMO terminal devices. In this article, OTA data throughputs of a two-antenna MIMO module with

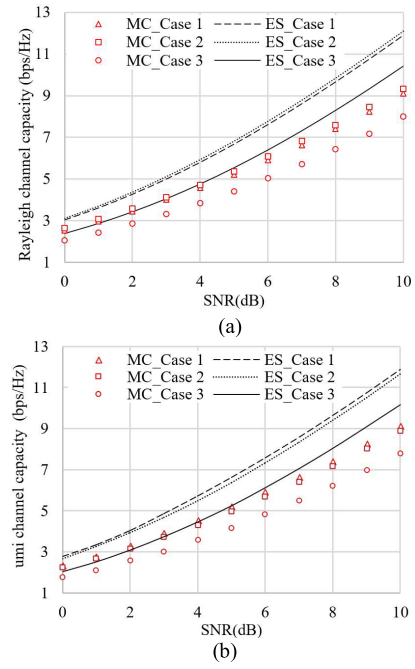


Fig. 5. Ergodic channel capacity of the three cases calculated by MC simulation and the upper bound ES under two channel models. (a) Rayleigh fading channel and (b) umi SCME channel.

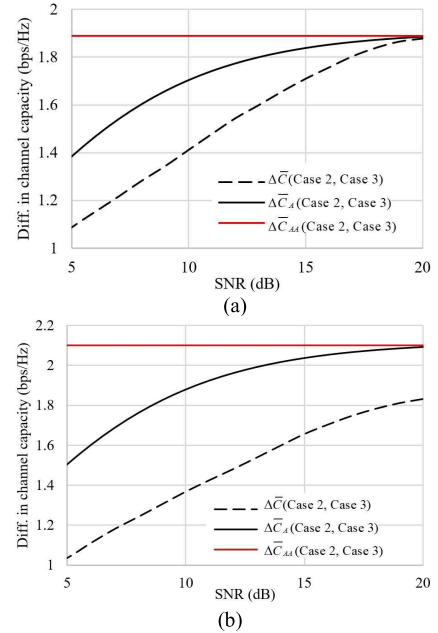


Fig. 6. Differences in ergodic channel capacities of Cases 2 and 3 calculated by accurate channel capacity $\Delta\bar{C}$ and two approximate capacity bond $\Delta\bar{C}_A$ and $\Delta\bar{C}_{AA}$ under two channel models. (a) Rayleigh fading channel and (b) umi SCME channel model.

different antenna configurations are measured in the in-house SATIMO MIMO-H MPAC channel emulator [23] to validate the consistency of ECC-M and OTA data throughput. Seven sets of two-element IFA antenna samples, namely, Cases a–g, are prepared with different mutual couplings and total efficiencies. The antennas are printed on an FR4 PCB board with relative permittivity of 4.6, thickness of 1 mm, and loss tangent

TABLE IV
DIMENSIONS FOR DIFFERENT ANTENNA SAMPLES

Dimensions (mm)	L1	L2	L3	L4	L5	L6	L7	L8
	140	75	7.5	20.6	4.1	8.9	2.5	2
	L9	L12	W1	W2				
Absorber dimensions (mm)	Case a/e/f/g		Case b		Case c		Case d	
	L10	L11	L10	L11	L10	L11	L10	L11
	0	0	4	6.5	7.2	6.5	11.5	6.5

TABLE V
DECOUPLING CAPACITOR VALUE, COUPLING, AND TOTAL EFFICIENCY FOR EACH TWO-ELEMENT ANTENNA CASE

Capacitor (pF)	Case a	Case b	Case c	Case d	Case e	Case f	Case g
	3.2	3.2	3.2	3.2	3	2	0
Coupling (dB)	-20	-21	-21	-22	-16	-13	-11
Efficiency (%)	80	63	50	40	76	68	63

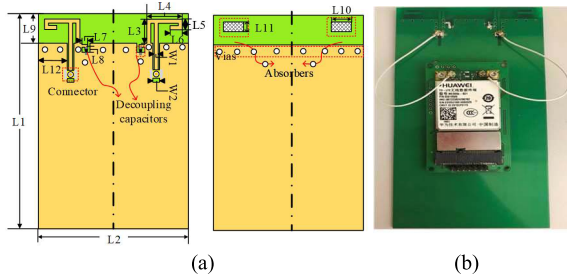


Fig. 7. (a) Two-element MIMO antenna for OTA measurement: front view and back view and (b) TD-LTE communication module connected by the two-element MIMO antenna for OTA measurement.

of 0.015. The layout of the antennas is sketched in Fig. 7(a). The antenna efficiency is altered by changing the size of a piece of absorber on the back of each IFA antenna, and mutual coupling between each pair of IFA antennas is controlled by adjusting a decoupling capacitor near each IFA antenna by following the self-curing decoupling technique [24]. The dimensions of the antenna samples are given in Table IV. The values of mutual coupling and total efficiency of each antenna case are listed in Table V together with the value of the decoupling capacitor. In all cases, the reflection coefficients of all the antennas are below -15 dB.

A commercial TD-LTE data communication module of HUAWEI ME909 is used as the wireless terminal device. A two-element antenna sample is connected to the module through a pair of short RF cables, as shown in Fig. 7(b). In the measurement, the operating frequency is set to LTE band 3 (1805–1880 MHz) with signal bandwidth of 10 MHz, which is supported by the communication module and the MPAC channel emulator. The maximum data rate is set to be 14.386 Mbps with modulation and coding scheme (MCS) index of 10 according to [10]. In this measurement, the umi SCME channel model is chosen. The data throughput is an average of the measured throughput values by rotating the wireless terminal device for every 45° in the horizontal plane.

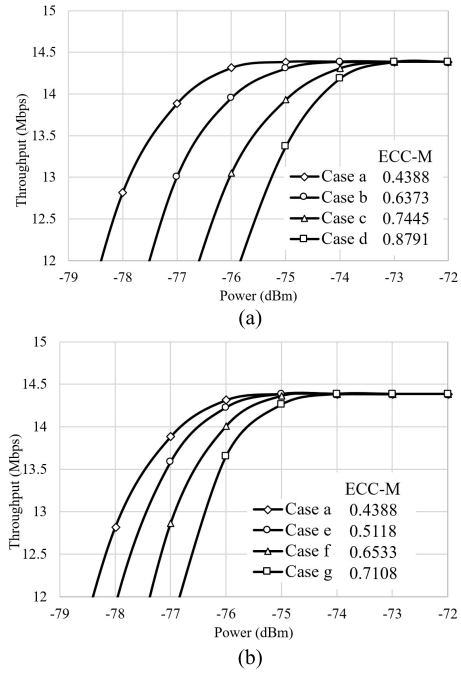


Fig. 8. Measured OTA data throughput for different antennas (a) total efficiencies and (b) mutual coupling.

The measured average data throughput versus input power (in dBm) for all cases is plotted in Fig. 8, in which the corresponding ECC-M calculated by (16) for each case is also inserted, showing very good consistency between the ECC-M values and measured OTA data throughput.

V. CONCLUSION

In this article, a capacity-oriented ECC, namely, ECC-M, is proposed to assess the performance of a multiple antenna system for a wireless mobile device. ECC-M is originated from the upper bound of the channel capacity. Therefore, the figure of merit not only accounts for the pattern correlation of each pair of antennas and the total efficiency of each antenna but also incorporates the channel model information. To provide a simple and analytical formula to calculate ECC-M for a realistic ray-based channel model, such as SCME models, a legitimate approximation of the pdf of AOA is provided, which enables the calculation of ECC-M with a ray-based realistic channel model in a simple integral form. It is demonstrated, through MC simulation and OTA throughput measurement, that the proposed ECC-M has a strong correlation with the ergodic channel capacity as well as the system OTA throughput. It is believed that the proposed ECC-M will find many practical applications in designing multiple antenna systems for MIMO enabled wireless mobile devices.

REFERENCES

[1] F. Rusek, D. Persson, B. K. Lau, E. G. Larsson, T. L. Marzetta, and F. Tufvesson, "Scaling up MIMO: Opportunities and challenges with very large arrays," *IEEE Signal Process. Mag.*, vol. 30, no. 1, pp. 40–60, Jan. 2013.
 [2] R. Vaughan and J. Andersen, "Antenna diversity in mobile communications," *IEEE Trans. Veh. Technol.*, vol. 36, no. 4 pp. 149–172, Nov. 1987.

- [3] S. Alamouti, "A simple transmit diversity technique for wireless communications," *IEEE J. Sel. Areas Commun.*, vol. 16, no. 8, pp. 1451–1458, Oct. 1998.
- [4] A. Forenza, M. R. McKay, A. Pandharipande, R. W. Heath, Jr., and I. B. Collings, "Adaptive MIMO transmission for exploiting the capacity of spatially correlated channels," *IEEE Trans. Veh. Technol.*, vol. 56, no. 2, pp. 619–630, Mar. 2007.
- [5] D. Sarkar and K. V. Srivastava, "Application of cross-correlation Greens function along with FDTD for fast computation of envelope correlation coefficient over wideband for MIMO antennas," *IEEE Trans. Antennas Propag.*, vol. 65, no. 2, pp. 730–740, Feb. 2017.
- [6] D. Sarkar and K. V. Srivastava, "Modified cross correlation Green's function with FDTD for characterization of MIMO antennas in nonuniform propagation environment," *IEEE Trans. Antennas Propag.*, vol. 66, no. 7, pp. 3798–3803, Jul. 2018.
- [7] R. Tian, B. K. Lau, and Z. Ying, "Multiplexing efficiency of MIMO antennas," *IEEE Antennas Wireless Propag. Lett.*, vol. 10, pp. 183–186, Mar. 2011.
- [8] D. Chizhik, F. Rashid-Farrokh, J. Ling, and A. Lozano, "Effect of antenna separation on the capacity of BLAST in correlated channels," *IEEE Commun. Lett.*, vol. 4, no. 11, pp. 337–339, Nov. 2000.
- [9] D. Hill, "Electromagnetic theory of reverberation chambers," NIST, Boulder, CO, USA, Tech. Rep., 1506, Dec. 1998.
- [10] CTIA. (May 2018). *Test Plan for 2x2 Downlink MIMO and Transmit Diversity Over-the-Air Performance*. Ver. 1.2. [Online]. Available: <https://api.ctia.org/>
- [11] W. Yu *et al.*, "Radiated two-stage method for LTE MIMO user equipment," *IEEE Trans. Electromagn. Compat.*, vol. 56, no. 6, pp. 1691–1696, Dec. 2014.
- [12] X. Chen, "Throughput modeling and measurement in an isotropic-scattering reverberation chamber," *IEEE Trans. Antennas Propag.*, vol. 62, no. 4, pp. 2130–2139, Apr. 2014.
- [13] W. Fan, P. Kyösti, J. Ø. Nielsen, and G. F. Pedersen, "Wideband MIMO channel capacity analysis in multiprobe anechoic chamber setups," *IEEE Trans. Veh. Technol.*, vol. 65, no. 5, pp. 2861–2871, May 2016.
- [14] X. Mei and K.-L. Wu, "Envelope correlation coefficient for multiple MIMO antennas of mobile terminals," in *Proc. IEEE Int. Symp. Antennas Propag. North Amer. Radio Sci. Meeting*, Montreal, QC, Canada, Jul. 2020, pp. 1597–1598.
- [15] C. E. Shannon, "A mathematical theory of communication," *Bell Syst. Tech. J.*, vol. 27, no. 3, pp. 379–423, 1948.
- [16] G. J. Foschini and M. J. Gans, "On limits of wireless communications in a fading environment when using multiple antennas," *Wireless Pers. Commun.*, vol. 6, pp. 311–335, Mar. 1998.
- [17] I. Csiszár and P. Narayan, "The capacity of the arbitrarily varying channel revisited: Positivity, constraints," *IEEE Trans. Inf. Theory*, vol. 34, no. 2, pp. 181–193, Jan. 1991.
- [18] *Spatial Channel Model for MIMO Simulations*, 3GPP document TR 25.996 V6.1.0, Sep. 2003. [Online]. Available: <http://www.3gpp.org/>
- [19] R. B. Ertel *et al.*, "Overview of spatial channel models for antenna array communication systems," *IEEE Pers. Commun.*, vol. 5, no. 1, pp. 10–22, Feb. 1998.
- [20] M. A. Jensen and J. W. Wallace, "A review of antennas and propagation for MIMO wireless communications," *IEEE Trans. Antennas Propag.*, vol. 52, no. 11, pp. 2810–2824, Nov. 2004.
- [21] *Analysis of DUT Pool 4 Test Results*, 3GPP, document R4-115655, Nokia, TSGRAN WG4 Meeting #61, USA, Nov. 2011.
- [22] D. J. Kraus and J. R. Marhefka, *Antennas for all Applications*, 3rd ed. New York, NY, USA: McGraw-Hill 2002, pp. 23–24.
- [23] Microwave Vision Group, FR. *StarMIMO: A MIMO Device End-to-End Test System*. Accessed: Sep. 2018. [Online]. Available: <https://www.mvg-world.com/>
- [24] J. Sui, Y. Dou, X. Mei, and K.-L. Wu, "Self-curing decoupling technique for MIMO antenna arrays in mobile terminals," *IEEE Trans. Antennas Propag.*, vol. 68, no. 2, pp. 838–849, Feb. 2020.



Xide Mei received the B.S. degree in electronic engineering from the University of Electronic Science and Technology of China, Chengdu, China, in 2015. He is currently pursuing the Ph.D. degree with The Chinese University of Hong Kong, Hong Kong.

His current research interests include antenna design, performance evaluation of terminal devices, and the design of multiple-input multiple-output antenna array by incorporating wireless channel models.



Ke-Li Wu (Fellow, IEEE) received the B.S. and M.Eng. degrees from the Nanjing University of Science and Technology, Nanjing, China, in 1982 and 1985, respectively, and the Ph.D. degree from Laval University, Quebec, QC, Canada, in 1989.

From 1989 to 1993, he was a Research Engineer with McMaster University, Hamilton, ON, Canada. He joined COM DEV (now Honeywell Aerospace), Cambridge, ON, Canada, in 1993, where he was a Principal Member of Technical Staff. Since 1999, he has been with The Chinese University of Hong Kong, Hong Kong, where he is currently a Professor and the Director of the Radiofrequency Radiation Research Laboratory. His current research interests include EM-based circuit domain modeling of high-speed interconnections, robot automatic tuning of microwave filters, decoupling techniques of multiple-input multiple-output (MIMO) antennas, and the Internet of Things (IoT) technologies.

Prof. Wu is a member of the IEEE MTT-8 Subcommittee. He was a recipient of the 1998 COM DEV Achievement Award and the Asia-Pacific Microwave Conference Prize twice in 2008 and 2012, respectively. He was an Associate Editor of the IEEE TRANSACTIONS ON MICROWAVE THEORY AND TECHNIQUES from 2006 to 2009.